



Proceedings of the
National Academy of Sciences
of the United States of America

RESEARCH ARTICLE



Light-triggered thermal conductivity switching in azobenzene polymers

Jungwoo Shin, Jaeuk Sung, Minjee Kang, Xu Xie, Byeongdu Lee, Kyung Min Lee, Timothy J. White, Cecilia Leal, Nancy R. Sottos, Paul V. Braun, and David G. Cahill

^a*Department of Materials Science and Engineering, University of Illinois at Urbana–Champaign, Urbana, IL 61801;*

^b*Materials Research Laboratory, University of Illinois at Urbana–Champaign, Urbana, IL 61801;*

^c*Beckman Institute for Advanced Science and Technology, University of Illinois at Urbana–Champaign, Urbana, IL 61801;*

^d*X-ray Science Division, Argonne National Laboratory, Argonne, IL 60439;*

^e*Materials and Manufacturing Directorate, Air Force Research Laboratory, Wright Patterson Air Force Base, OH 45433*

– Hide authors and affiliations

PNAS March 26, 2019 116 (13) 5973–5978; first published March 8, 2019; <https://doi.org/10.1073/pnas.1817082116>

Edited by Timothy M. Swager, Massachusetts Institute of Technology, Cambridge, MA, and approved February 12, 2019 (received for review October 19, 2018)

PDF

Help

This article has a Correction. Please see:

Correction for Shin et al., Light-triggered thermal conductivity switching in azobenzene polymers - April 15, 2019

Article

Figures & SI

Info & Metrics

PDF

Significance

Heat is carried as diffusion of vibrational modes in insulating polymers, a process that is highly dependent on the macromolecular ordering of a polymer. As a result, changes in macromolecular ordering have potential to significantly change the thermal transport property of a polymer. Here, we design and synthesize a thermally switchable azobenzene polymer that exhibits a reversible crystal-to-liquid transition in response to UV and visible light. By driving a transition between the planar (*trans*) and nonplanar (*cis*) conformational states of azobenzene moieties attached to the polymer, we modulate interchain π - π bonding, resulting in fast and reversible thermal and structural transitions. This work unravels the pathway of crystal-to-liquid transitions of the azobenzene polymer and the resulting thermal and physical property changes.

Abstract

Materials that can be switched between low and high thermal conductivity states would advance the control and conversion of thermal energy. Employing in situ time-domain thermoreflectance (TDTR) and in situ synchrotron X-ray scattering, we report a reversible, light-responsive azobenzene polymer that switches between high ($0.35 \text{ W m}^{-1} \text{ K}^{-1}$) and low thermal conductivity ($0.10 \text{ W m}^{-1} \text{ K}^{-1}$) states. This threefold change in the thermal conductivity is achieved by modulation of chain alignment resulted from the conformational transition between planar (*trans*) and nonplanar (*cis*) azobenzene groups under UV and green light illumination. This conformational transition leads to changes in the π - π stacking geometry and drives the crystal-to-liquid transition, which is fully reversible and occurs on a time scale of tens of seconds at room temperature. This result demonstrates an effective control of the thermophysical properties of polymers by modulating interchain π - π networks by light.

polymer thermal conductivity phase transition thermal switch azobenzene

At the most fundamental level, the chemical structure of a polymer dictates its properties (1). Thus, stimuli-modulated reversible chemical transitions can drive reversible property changes (2). Light (3–5), electric (6) and magnetic (7) fields, temperature (8), redox reactions (9), mechanical force (10), and changes in pH (11) have all been demonstrated as triggers for reversible physical and chemical property transitions for applications of polymers in sensing, drug delivery, actuation, and self-healing (12–14). However, no polymers have been shown to undergo extreme changes in macromolecular ordering, e.g., crystal-to-liquid, in response to nonthermal stimuli. Here, we describe a photoresponsive azobenzene-based polymer (azopolymer) exhibiting an unprecedented reversible crystal-to-liquid transition driven by UV (375 nm) and green (530 nm) light-triggered modulation of interchain π - π interactions. This is an observation of a reversible phototriggered crystal-to-liquid transition in a polymeric material. In conjunction with the structural transition, the polymer exhibits a notable thermal conductivity contrast, r , between the crystal, Λ_{high} and liquid, Λ_{low} states, with $r = \Lambda_{\text{high}}/\Lambda_{\text{low}} \sim 3.5$. In comparison, r of a giant-magneto-thermorestrictive material is ~ 1.8 (15); r of a liquid crystal network switched with a magnetic field is ~ 1.5 (16); and r of electrochemically lithiated/delithiated Li_xCoO_2 is ~ 1.5 (17, 18). Our results demonstrate powerful control of the thermophysical properties of polymers by light. The fast (seconds),

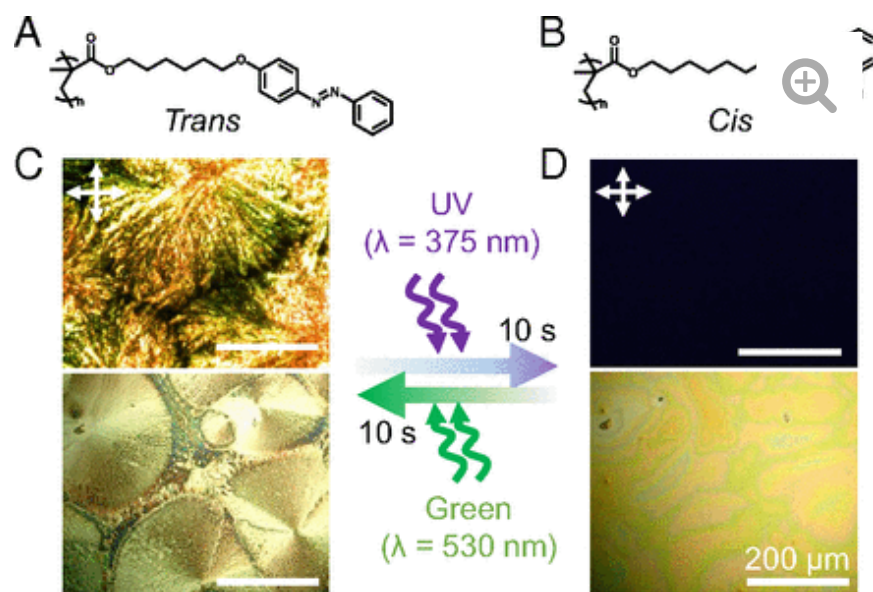
reversible crystal-to-liquid transition may also provide a class of polymers engineered to switch physical, optical, and thermal properties on demand, which may enable controlled molecular release, mechanical bonding, and reconfigurable thermal routing.

Results and Discussion

Light-Triggered Phase Transition.

We hypothesized that photoisomerization of azobenzene groups attached to a polymer backbone could be used to modulate interchain bonding strength, driving nonthermal switching of polymers between crystalline and amorphous/fluidic states in a fast and reversible manner. We based our hypothesis on prior works showing that small molecule azobenzenes (**19**, **20**) could undergo optically triggered crystal-to-crystal and crystal-to-liquid transitions, and azobenzene-containing polymers underwent optically triggered glass-to-liquid transitions (**21**). This phase-transition mechanism of azobenzene molecules has been studied to optically trigger the phase transition of organic phase-change materials in thermal energy storage systems (**22**, **23**).

Here, we synthesize and investigate both the structural and thermal properties of a photoresponsive azobenzene-based polymer (azopolymer). **Fig. 1** shows the chemical structure of the azopolymer we synthesized, as well as optical microscopy (OM) and cross-polarized OM (POM) images of a spin-coated azopolymer film in the *cis* (after UV exposure) and *trans* (after green light exposure or time) states (sample preparation details are provided in the **Method** and **SI Appendix**).



PDF

Help

[Download figure](#)[Open in new tab](#)[Download powerpoint](#)

Fig. 1.

Light-triggered phase transition of azopolymer. (A and B) *Trans*-azopolymer (A) and *cis*-azopolymer (B) structures. (C and D) Corresponding appearances of *trans*-azopolymer (C) and *cis*-azopolymer (D) films under cross-polarized OM (*Upper*) and OM under continuous UV and green light illuminations (*Lower*) (Movie S1). (Scale bars, 200 μm .)

[Open in new tab](#)[Download original movie](#)**Movie S1.**

Light-triggered reversible crystal-to-liquid transition of a spin-coated azopolymer film on the Al/polyimide/sapphire substrate under UV (375 nm) (00:00:03~) and green (530 nm) light illumination (00:00:26~) (630 mW cm^{-2}).

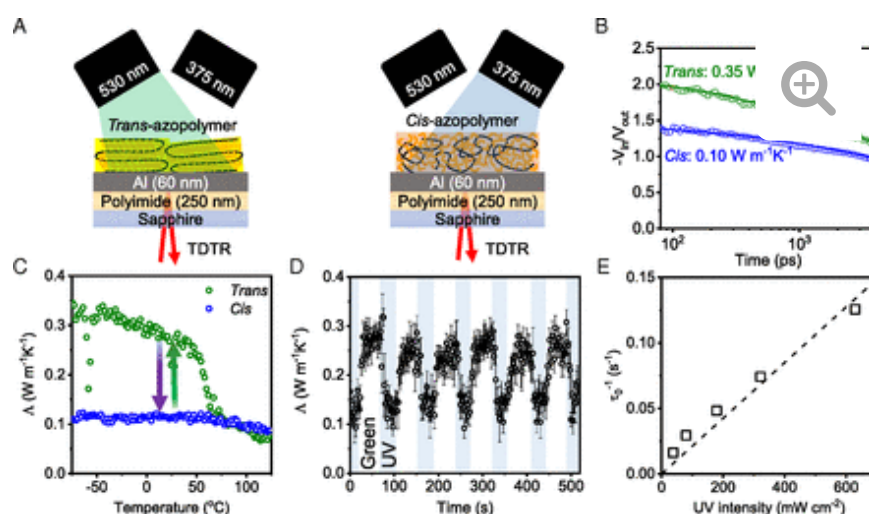
[PDF](#)[Help](#)

Starting from the crystalline ground state (**Fig. 1A**), UV light triggers a *trans*-to-*cis* photoisomerization leading to melting of the polymer (**Fig. 1B**). Upon green light triggered reconversion of the *cis*-azobenzene groups to *trans*-azobenzene, the polymer returns to the crystalline state (at room temperature in the dark, the *cis*-to-*trans* isomerization will also take place over the course of several hours). The light-triggered melting and crystallization is a direct result of differences in the stacking of the planar *trans*- and nonplanar *cis*-states of the azobenzene group. The planar *trans*-azobenzene readily undergoes π - π stacking, while the bent *cis*-azobenzene, in which the two phenyl rings align in different planes (**24**), does not (**19**). As shown in the OM and POM images (**Fig. 1 C and D**), spherulites in the crystalline *trans*-azopolymer film disappear upon exposure to UV light and reappear upon exposure to

green light. Under our UV and green light illumination conditions, the melting and crystallization are complete within 10 s (Movie S1 and *SI Appendix*, Figs. S1 and S2). Hereafter, we refer to the crystalline and liquid states of azopolymer as *trans*- and *cis*-azopolymer, respectively.

Thermal Conductivity Switching.

Across the crystal-to-liquid transition, the most significant property change observed, other than the crystal-liquid transition, is a threefold change in the thermal conductivity in a matter of seconds at room temperature. We measured the dependence of the out-of-plane thermal conductivity of the azopolymer film on exposure to UV and green light using in situ time-domain thermoreflectance (TDTR) (16, 25). **Fig. 2A** shows a schematic illustration for the experimental configuration of in situ TDTR measurements for azopolymer/Al/polyimide/sapphire samples under green and UV light illumination. **Fig. 2B** shows measured and fitted TDTR curves for *trans*- and *cis*-azopolymer films after green and UV light illumination. The thermal conductivity reversibly switches between $0.35 \pm 0.05 \text{ W m}^{-1} \text{ K}^{-1}$ in *trans*-azopolymer to $0.10 \pm 0.02 \text{ W m}^{-1} \text{ K}^{-1}$ in *cis*-azopolymer. These values are within the values expected for polymers: for example, the thermal conductivity of polyethylene varies from $0.1 \text{ W m}^{-1} \text{ K}^{-1}$, when randomly oriented to $90 \text{ W m}^{-1} \text{ K}^{-1}$ along the draw direction of a highly oriented crystalline fiber (26, 27).



[Download figure](#)

[PDF](#)

[Help](#)

[Open in new tab](#)

[Download powerpoint](#)

Fig. 2.

Thermal conductivity switching of azopolymer. (A) Schematic illustration for in situ TDTR measurements for an azopolymer film under green and UV light illumination. (B) Measured and fitted TDTR data for *trans*- and *cis*-azopolymer films after green and UV light illumination, respectively. (C) Temperature-dependent thermal conductivity of *trans*- and *cis*-azopolymer films. (D) Thermal conductivity of the azopolymer film under alternating green and UV light illumination. The reversible *trans*-to-*cis* transitions between the crystalline and liquid states occur within 10 s under UV and green light illumination (320 W cm^{-2}). Error bars represent temporal signal fluctuations and experimental uncertainty. (E) Thermal conductivity switching rate τ_0^{-1} of azopolymer film with increasing UV intensity.

Fig. 2C shows temperature-dependent thermal conductivity of *trans*- and *cis*-azopolymers. **Fig. 2D** shows the thermal conductivity of the azopolymer under alternating UV and green light illumination; 90% of the change in thermal conductivity occurs within a few tens of seconds when the light intensity is 320 mW cm⁻². The rate of thermal conductivity switching, τ_0^{-1} , which is the rate to achieve 90% of the total thermal conductivity change, increases from 0.016 to 0.126 s⁻¹ as the UV light intensity increases from 38 to 630 mW cm⁻² (**Fig. 2E**). The thermal conductivity of the liquid state azopolymer measured by TDTR agrees with the value obtained from a frequency-domain probe beam deflection (FD-PBD) method (*SI Appendix*, Fig. S3) (**28**).

UV-visible spectroscopy and differential scanning calorimetry (DSC) measurements confirm the *trans-cis* photoisomerization (*SI Appendix*). We observe an appearance of a glass transition temperature ($T_{g,cis}$) at -48 °C after exposure to UV light, which disappears upon exposure to green light. This transition temperature is markedly lower than the temperature of a small endothermic inflection in the DSC data at 31 °C, which we interpret as T_g of residual amorphous *trans*-azopolymer. (The *trans*-azopolymer melting point is 80 °C.) Previous studies of polymers with similar azobenzene side-chain structures in *trans* states have reported glass-transition temperatures in the range of 35 < T_g < 80 °C (**29–31**). We note that similar large shifts in T_g as a function of isomer state have been previously observed in polybutadiene ($\Delta T_g \sim 90$ °C) (**32**) and azobenzene functionalized polymers ($\Delta T_g \sim 60$ °C) (**21**). All measured physical parameters, including the molecular weight, the polydispersity indices (PDIs), heat capacity per unit volume (C), T_g , T_m , and longitudinal and transverse speed of sounds (V_l and V_t) and elastic moduli (C_{11} and C_{44}) for *trans*- and *cis*-azopolymers, are described in *SI Appendix*, Figs. S4–S7 and summarized in **Table 1**.

Table 1.Physical properties of *trans*- and *cis*-azopolymer[VIEW INLINE](#) [VIEW POPUP](#)

While C can have a significant impact on the thermal conductivity, we observe that C is only ~10% greater in the amorphous state than the crystalline state, and yet the crystalline *trans*-azopolymer exhibits an 80% higher thermal conductivity than the amorphous *trans*-azopolymer ($\Lambda_{\text{amorphous}} = 0.19 \text{ W m}^{-1} \text{ K}^{-1}$) (*SI Appendix*, Fig. S8), suggesting that crystallinity plays the dominant role in the change in thermal conductivity. We speculate that the higher thermal conductivity of crystalline *trans*-azopolymer is the result of stronger dispersion and longer lifetimes of vibrational modes created by the out-of-plane alignment of side chains with planar azobenzene groups. The thermal conductivity contrast of azopolymer, $r \sim 3.5$, is similar to what is observed at the melting transition of *n*-alkanes ($n = 9 \sim 19$) with $r \sim 2 \sim 3$ (**33, 34**). This comparison supports our assertion that we can attribute the enhancement in the out-of-plane thermal conductivity to the side-chain alignment where the fully stretched side-chain length (21 Å) is comparable to *n*-alkanes with $n = 16\text{--}17$.

Due to the limitations in the experiments associated with a very low sensitivity of the TDTR signals to in-plane thermal conductivity, our experimental data are limited to the out-of-plane thermal conductivity of azopolymer films. Nevertheless, we expect that the in-plane thermal conductivity of azopolymer film is

lower than the out-of-plane thermal conductivity since the direction of thermal conduction is normal to the aligned side chains where most of heat would be carried by interchain interaction across the side-chain networks.

Macromolecular-Ordering Transitions.

Polymer films with azobenzene side-chain groups often form smectic or lamellar structures with an out-of-plane side-chain arrangement (**35**, **36**), exhibiting characteristic side-chain interdigitation due to the π - π stacking of azobenzene groups (**37**). Upon UV light illumination, these interchain π - π interactions decrease dramatically with the torsional rotation of the azobenzene groups (**19**). **Fig. 3A** illustrates a possible mechanism for crystal-to-liquid transition, associated with disruption of the π - π -stacked azobenzene groups in azopolymer during the *trans*-to-*cis* isomerization. Upon UV excitation, the *trans*-azobenzene groups transform to nonplanar *cis*-azobenzene isomers with various (C-N = N-C) dihedral angles between the two phenyl rings. This torsional rotation of the azobenzene groups causes a steric hindrance for azobenzene π - π stacking (**24**). As the population of the *cis*-isomer grows, the azobenzene stacking decreases, and long-range crystalline order is lost (**19**). Upon exposure to the green light (*cis*-to-*trans* transition), crystalline order is recovered by stacking of the *trans*-azobenzene groups.

[PDF](#)[Help](#)[Download figure](#)[Open in new tab](#)[Download powerpoint](#)

Fig. 3.

Evolution of π - π stacking of azobenzene groups during *trans*-to-*cis* photoisomerization. (A) Schematic illustration of the conformation changes of the azopolymer driven by photoisomerization. (B) 2D GIWAXS diffraction pattern of the *trans*-azopolymer film. (C) Azimuth integrated in situ transmission WAXS intensity of the azopolymer during the *trans*-to-*cis* transition driven by UV illumination (630 mW cm^{-2}). (D) $d_{\pi-\pi}$ and FWHM of the π - π stacking peak as a function of *trans*-to-*cis* photoisomerization time. Error bars represent the uncertainty of q . This time-dependent plot represents the $d_{\pi-\pi}$ diffraction shift in C.

We performed in situ synchrotron grazing-incidence wide-angle X-ray scattering (GIWAXS), wide-angle X-ray scattering (WAXS), grazing-incidence small-angle X-ray scattering (GISAXS), and small-angle X-ray scattering (SAXS) measurements to test this hypothesis and study the temporal evolution of short- and long-range macromolecular structure created by UV and green light illumination. **Fig. 3B** shows a 2D GIWAXS diffraction pattern of a *trans*-azopolymer film. Two sets of diffraction rings can be observed. One corresponds to in-plane diffraction associated with the lateral side-chain interdigitation of azobenzene π - π stacking ($d_{\pi-\pi}$) at $q = 1.68\text{--}1.78 \text{ \AA}^{-1}$. The second arises from out-of-plane diffraction at integral multiples of $q_z = 0.233 \text{ \AA}^{-1}$, consistent with a 2.7-nm (001) lamellar spacing of the azopolymers. The diffraction changes associated with $d_{\pi-\pi}$ and lamellar spacing represent macromolecular ordering of the azopolymer at different length scales. **Fig. 3C** shows the time-dependent, azimuth-integrated WAXS signal intensity. Under UV light illumination, the $d_{\pi-\pi}$ peak gradually broadens and shifts to lower q , while the unit cell lattice (010) reflection remains at $q = 1.22 \text{ \AA}^{-1}$. After ~ 20 s of UV illumination, the $d_{\pi-\pi}$ peak fades, followed by damping of the (010) peak, leaving only a broad diffuse scattering ring. **Fig. 3D** shows $d_{\pi-\pi}$ spacing and the $d_{\pi-\pi}$ peak full width at half-maximum (FWHM) during the *trans*-to-*cis* photoisomerization. Subsequent green light illumination triggers a *cis*-to-*trans* transition in which all diffraction patterns reappear, indicating recovery of the interdigitated structure. The time scale of the phase transition corresponds to the time scale of the thermal conductivity switching observed in TDTR measurements (*SI Appendix*, Figs. S9–S11).

In addition to the short-range order-disorder transition of side-chain azobenzene groups revealed by the WAXS measurements, we performed in situ SAXS to study the long-range order-disorder transition of the azopolymer backbone under UV and green light illumination. **Fig. 4A** shows a 2D GISAXS diffraction pattern of a *trans*-azopolymer film. We observe integral multiples of $q_z = 0.233 \text{ \AA}^{-1}$ and $q_z = 0.224 \text{ \AA}^{-1}$, consistent with a double periodic array at short (001)_s and long (001)_l spacings for *trans*-azopolymer lamellae.

PDF

Help



Download figure

Open in new tab

Download powerpoint

Fig. 4.

Phototriggered reversible lamellar crystallization pathway. (A) 2D GISAXS diffraction pattern of the *trans*-azopolymer film. (B) Azimuth integrated in situ transmission SAXS intensity of azopolymers during *trans*-to-*cis* photoisomerization (UV light). (C) Azimuth integrated transmission SAXS intensity of azopolymers during the *cis*-to-*trans* photoisomerization (green light). (D) Schematic showing the suggested crystallization pathway under green light illumination (right to left). (D, *i-iii*) Randomly distributed *cis*-azopolymer chains (*i*) initially form an intermediate phase consisting of noninterdigitated polymer clusters (*ii*), followed by the formation of the interdigitated structure with long (001)_l and short (001)_s spacings (*iii*).

PDF

Help

Fig. 4 B and C shows the changes of azimuth-integrated SAXS intensity of azopolymers during *trans*-to-*cis* and *cis*-to-*trans* transitions. The interdigitated (001) and (002) peaks decay under UV illumination in ~10 s. Crystallization into the lamellar structure occurs under subsequent green light illumination on a comparable time scale. Before formation of the final lamellar structure, we observe a transient diffraction peak at $q = 0.189 \text{ \AA}^{-1}$, which can be attributed to an intermediate phase consisting of a weakly ordered structure ($d = 3.3 \text{ nm}$) that does not give rise to higher-order diffraction peaks. The diffraction peak of this intermediate phase decays rapidly as the fully interdigitated (001)_s and partially interdigitated (001)_l peaks grow in intensity (*SI Appendix*, Figs. S12–S14). The transient nature of the intermediate phase before the formation of the lamellar structure supports a crystallization pathway that passes through a weakly ordered phase. We speculate that in this intermediate state, side chains form a noninterdigitated structure during the *cis*-to-*trans* isomerization before forming the interdigitated structure. After the

azopolymer chains are interdigitated at the nucleation site, they exhibit outward growth of the spherulite structure (**Fig. 1**). **Fig. 4D** is a schematic illustration of the assembly and crystallization process outlined here. The intensity of the $(001)_s$ peak is an order of magnitude higher than the $(001)_l$ peak, suggesting that $(001)_s$ is the most dominant structure. This split peak can be attributed to the two distinct populations of lamellar spacings originating from slightly different azobenzene interdigitation configurations (**37, 38**) (*SI Appendix*, Figs. S15 and S16).

Conclusion.

In summary, we observe reversible crystal–liquid transitions in an azopolymer, which occur on the order of 10 s with a UV and green light under illumination intensities on the order of 100 mW cm^{-2} . This transition is associated with a threefold change in thermal conductivity. UV light illumination induces a transition in the azobenzene side chains from the planar *trans* state to the nonplanar *cis* state; green light illumination reverses this transition. The torsional rotation of the phenyl rings in *cis*-azobenzene disrupts π - π interactions between the azobenzene groups, resulting in formation of an isotropic liquid with a thermal conductivity of $0.10 \text{ W m}^{-1} \text{ K}^{-1}$. Subsequent green light illumination induces crystallization of *trans*-azopolymer, which is found to have a thermal conductivity of $0.35 \text{ W m}^{-1} \text{ K}^{-1}$ and consists of crystals containing interdigitated aligned planar-azobenzene side chains. Excitingly, we find that the conformational state of specific functional groups on polymer chains regulates not only short- and long-range ordering but also the thermal transport properties of the polymer.

Methods

Sample Preparation.

All materials were purchased from Sigma-Aldrich. 4-Phenylazophenol (98%), methacryloyl chloride (97%), 6-bromo-1-hexanol (97%), and cyanoisopropyl dithiobenzoate were used as received. 2,2'-Azobisisobutyronitrile (98%) was recrystallized in chloroform before use. A complete synthetic procedure for azopolymer is available in *SI Appendix*.

We prepared ~ 280 -nm thick, *trans*-azopolymer thin films by spin-coating 5 wt% azopolymer dissolved in a mixture of cyclopentanone and cyclohexane (9:1 weight ratio) on Al/polyimide/sapphire substrates. The substrates were first prepared by spin-coating a 250-nm polyimide film on a sapphire wafer, followed by a 60-nm Al film deposition using magnetron sputtering. The purpose of the polyimide film is to reduce heat flow between the Al transducer and the sapphire substrate and thereby to increase the sensitivity of the TDTR measurements to the thermal conductivity of the azopolymer layer. The same specimens were used throughout the in situ OM, in situ TDTR, and in situ synchrotron X-ray scattering measurements.

OM.

The OM images and movies were recorded using a VHX-5000 series Keyence Digital Microscope at $200\times$ magnification. The phase transition of azopolymers was characterized under green (530 nm) and UV (375 nm) light illumination. We used collimated LEDs with wavelengths of 530 and 375 nm for green and UV light sources, respectively (M530L3 and M375L3; Thorlabs). We focused the light on a 0.16-cm^2

area. The illuminated light intensity was controlled between 38 and 630 mW cm⁻² using a variable power controller LEDD1B (Thorlabs). Movies S1 and S2 show the phase transition of the spin-coated *trans*-azopolymer film and powder under UV and green light illumination (630 mW cm⁻²).

Open in new tab

Download original movie

PDF

Movie S2.

Light-triggered reversible crystal-to-liquid transition of azopolymer powder on a SiO₂ substrate under UV (375 nm) (00:00:07~) and green (530 nm) light illumination (00:01:07~) (630 mW cm⁻²).

TDTR.

We performed in situ TDTR measurements with our two-tint pump-probe Ti-sapphire laser system to heat and sense the temperature excursions of the azopolymer/Al (60 nm)/polyimide (250 nm)/sapphire samples (**25, 39**). We used a bidirectional temperature model in which the pump and probe beams arrive from and reflect through the transparent sapphire substrate side of the sample (**16**). We collected in-phase voltage (V_{in}) and out-of-phase voltage (V_{out}) from a radio frequency lock-in amplifier synchronized to the modulation of the intensity of the pump beam at $f = 1.12$ and 11 MHz. The temperature-dependent thermal conductivities of *trans*- and *cis*-azopolymers were measured using a temperature-controlled

Instec Hot/Cold stage having an optical window with the heating and cooling rates of $10\text{ }^{\circ}\text{C min}^{-1}$ under continuous green and UV illuminations (630 mW cm^{-2}). We used the measured ratio of V_{in} and V_{out} with a varying time delay between pump and probe pulses from 80 ps and 3.6 ns to calculate the thermal properties of *trans*- and *cis*-azopolymers. The $1/e^2$ intensity radius was $10\text{ }\mu\text{m}$, and the intensities of the pump and probe beam were 5 and 3 mW, respectively. The steady-state temperature rise, ΔT_{SS} , of the probed region was $\sim 10\text{ K}$. The thermal penetration depths are $\sqrt{\Lambda/(f\pi C)} \approx 55\text{--}75\text{ nm}$ at 11 MHz and $180\text{--}240\text{ nm}$ at 1.12 MHz. These penetration depths are much smaller than the size of the focused beam, and consequently, the TDTR measurements of the azopolymer layer are only sensitive to the thermal conductivity in the direction normal to the surface. At $f = 11\text{ MHz}$, the bidirectional heat flow model is sensitive to the thermal effusivity, $e = \sqrt{\Lambda C}$, where Λ and C are the thermal conductivity and heat capacity per unit volume of the azopolymer, respectively. C is independently determined by combining measurements of a 280-nm thick azopolymer film using modulation frequencies of 10.1 and 1.12 MHz at room temperature (40). To measure changes in thermal conductivity during the crystal-to-liquid phase transition, we fixed the delay time at 100 ps and continuously measured V_{in} and V_{out} under UV and green light illumination. The partial loss of thermal conductivity was attributed to incomplete crystallization due to insufficient time of illumination and the steady-state temperature rise during in situ TDTR measurements.

DSC.

DSC was performed to study the phase-transition temperature of the azopolymer with *trans* and *cis* conformational states of the attached azobenzene groups. The DSC measurements were performed using a TA Instrument Q20 Differential Scanning Calorimeter equipped with a Liquid Nitrogen Cooling System. Tzero aluminum pan and lids were used as sample containers. Al_2O_3 was used as a reference material for calculating the specific heat of azopolymers. Dry nitrogen was used as a sample purge gas. The heating and cooling rates were $10\text{ }^{\circ}\text{C min}^{-1}$. We determined the glass transition temperature (T_g), melting temperature (T_m), and crystallization temperature (T_c) of the *trans*- and *cis*-azopolymers from the inflection points in the DSC data.

Speed of Sound Measurements.

Transverse (V_t) and longitudinal (V_l) speeds of sound were measured using picosecond acoustic and surface acoustic wave measurements for crystalline azopolymer and picosecond interferometry for liquid azopolymer using a TDTR setup (41, 42). V_l was calculated from the acoustic echoes from Al/azopolymer film interphase using the relationship $V_l = 2h/\Delta t$, where h is the thickness of azopolymer and Δt is the time between echoes. V_t was calculated by generating and measuring surface acoustic waves using a periodic elastomeric PDMS mask on *trans*-azopolymer film. The longitudinal (C_{11}) and transverse (C_{44}) elastic moduli were calculated as $C_{11} = \rho V_l^2$ and $C_{44} = \rho V_t^2$. For liquid-state azopolymer, V_l of liquid is given by $V_l = v_p/(2\lambda n_l)$, where v_p is the in-phase TDTR probe beam oscillation frequency, λ is the wavelength of light, and n_l is the refractive index of liquid.

Synchrotron X-Ray Scattering.

PDF

Help

To study macromolecular order and the effect of light on chain alignment, we brought the azopolymer/Al/polyimide/sapphire samples to the 12-ID-B and 12-ID-C beamlines at the Advanced Photon Source at the Argonne National Laboratory for in situ synchrotron X-ray scattering measurements. We carried out GIWAXS, transmission WAXS, GISAXS, and transmission SAXS to study the short- and long-range macromolecular structural evolution of azopolymers under illumination by UV and green light. Samples were probed using 13.3 keV (12-ID-B) and 18 keV (12-ID-C) X-rays. The X-ray beam width was 200 μm . The samples were placed on a temperature-controlled stage at a temperature of 25–30 °C. The UV and green LEDs were mounted 15 cm above the sample stage. The LEDs were remotely controlled during X-ray scattering measurements. The data collection time of the detector was set at 0.5 s for the GISAXS, SAXS, and GIWAXS experiments and 1 s for the WAXS experiments. The time intervals between each data collection were 1 and 3 s for the SAXS and WAXS measurements, respectively.

Data Availability.

We deposited raw synchrotron X-ray scattering datasets in the Globus Materials Data Facility (MDF) Open, dx.doi.org/doi:10.18126/M2VH2X (43). All data are available in the main text, the *SI Appendix*, and MDF Open.

Acknowledgments

Sample preparation and characterization was performed at the Materials Research Laboratory and the Beckman Institute for Science and Technology at the University of Illinois at Urbana–Champaign. This work was supported by the National Science Foundation Engineering Research Center for Power Optimization of Electro-Thermal Systems, with Cooperative Agreement EEC-1449548, and Air Force Office of Scientific Research Grant FA9550-16-1-0017. This research used resources of the Advanced Photon Source, a US Department of Energy (DOE) Office of Science User Facility operated for the DOE Office of Science by Argonne National Laboratory under Contract DE-AC02-06CH11357. Authors declare no competing interests.

[PDF](#)[Help](#)

Footnotes

↵¹J. Shin and J. Sung contributed equally to this work.

↵²To whom correspondence may be addressed. Email: pbraun@illinois.edu or d-cahill@illinois.edu.

Author contributions: J. Shin, J. Sung, K.M.L., and T.J.W. designed research; J. Shin, J. Sung, M.K., and B.L. performed research; J. Shin, X.X., and D.G.C. contributed new reagents/analytic tools; J. Shin, J. Sung, M.K., B.L., C.L., N.R.S., P.V.B., and D.G.C. analyzed data; and J. Shin, J. Sung, P.V.B., and D.G.C. wrote the paper.

The authors declare no conflict of interest.

This article is a PNAS Direct Submission.

Data deposition: The raw synchrotron X-ray scattering datasets of the 2D diffraction images reported in this paper have been deposited in Globus MDF Open, dx.doi.org/doi:10.18126/M2VH2X.

This article contains supporting information online at www.pnas.org/lookup/suppl/doi:10.1073/pnas.1817082116/-/DCSupplemental.

Published under the PNAS license.

References

1. †Koros WJ, Burgess SK, Chen Z (2015) Polymer transport properties. *Encyclopedia of Polymer Science and Technology*. Available at <https://doi.org/10.1002/0471440264.pst376.pub2>. Accessed March 4, 2019. [Google Scholar](#)
2. †Stuart MAC, et al. (2010) Emerging applications of stimuli-responsive polymer materials. *Nat Mater* **9**:101–113. [CrossRef](#) [PubMed](#) [Google Scholar](#)
3. †White TJ, Broer DJ (2015) Programmable and adaptive mechanics with liquid crystal polymer networks and elastomers. *Nat Mater* **14**:1087–1098. [CrossRef](#) [PubMed](#) [Google Scholar](#)
4. †Burnworth M, et al. (2011) Optically healable supramolecular polymers. *Nature* **472**:334–337. [CrossRef](#) [PubMed](#) [Google Scholar](#)
5. †Suzuki A, Tanaka T (1990) Phase-transition in polymer gels induced by visible-light. *Nature* **346**:345–347. [CrossRef](#) [Google Scholar](#)
6. †Tanaka T, Nishio I, Sun ST, Ueno-Nishio S (1982) Collapse of gels in an electric field. *Science* **218**:467–469. [Abstract/FREE Full Text](#) [Google Scholar](#)
7. †Thévenot J, Oliveira H, Sandre O, Lecommandoux S (2013) Magnetic responsive polymer composite materials. *Soc Rev* **42**:7099–7116. [Google Scholar](#)
8. †Heskins MG, Guillet JE (1968) Solution properties of poly(N-isopropylacrylamide). *J Macromol Sci Chem* **2**:1441–1455. [CrossRef](#) [Google Scholar](#)
9. †Gandhi MR, Murray P, Spinks GM, Wallace GG (1995) Mechanism of electromechanical actuation in polypyrrole. *Synth Met* **73**:247–256. [CrossRef](#) [Google Scholar](#)
10. †Davis DA, et al. (2009) Force-induced activation of covalent bonds in mechanoresponsive polymeric materials. *Nature* **459**:68–72. [CrossRef](#) [PubMed](#) [Google Scholar](#)

PDF

Help

Chem

11. †Dai S, Ravi P, Tam KC (2008) pH-Responsive polymers: Synthesis, properties and applications. *Soft Matter* **4**:435–449. [Google Scholar](#)
12. †de Las Heras Alarcon C, Pennadam S, Alexander C (2005) Stimuli responsive polymers for biomedical applications. *Chem Soc Rev* **34**:276–285. [CrossRef](#) [PubMed](#) [Google Scholar](#)
13. †Zhai L (2013) Stimuli-responsive polymer films. *Chem Soc Rev* **42**:7148–7160. [Google Scholar](#)
14. †Wei ML, Gao YF, Li X, Serpe MJ (2017) Stimuli-responsive polymers and their applications. *Polym Chem Uk* **8**:127–143. [Google Scholar](#)
15. †Kimling J, et al. (2015) Spin-dependent thermal transport perpendicular to the planes of Co/Cu multilayers. *Phys Rev B Condens Matter Mater Phys* **91**:144405. [Google Scholar](#)
16. †Shin J, et al. (2016) Thermally functional liquid crystal networks by magnetic field driven molecular orientation. *ACS Macro Lett* **5**:955–960. [Google Scholar](#)
17. †Cho J, et al. (2014) Electrochemically tunable thermal conductivity of lithium cobalt oxide. *Nat Commun* **5**:4035. [Google Scholar](#)
18. †Wehmeyer G, Yabuki T, Monachon C, Wu JQ, Dames C (2017) Thermal diodes, regulators, and switches: Physical mechanisms and potential applications. *Appl Phys Rev* **4**:041304. [Google Scholar](#)
19. †Hoshino M, et al. (2014) Crystal melting by light: X-ray crystal structure analysis of an azo crystal showing photoinduced crystal-melt transition. *J Am Chem Soc* **136**:9158–9164. [Google Scholar](#)
20. †Bushuyev OS, Corkery TC, Barrett CJ, Friscic T (2014) Photo-mechanical azobenzene cocrystals and in situ X-ray diffraction monitoring of their optically-induced crystal-to-crystal isomerisation. *Chem Sci (Camb)* **5**:3158–3164. [Google Scholar](#)
21. †Zhou H, et al. (2017) Photoswitching of glass transition temperatures of azobenzene-containing polymers induces reversible solid-to-liquid transitions. *Nat Chem* **9**:145–151. [Google Scholar](#)
22. †Han GGD, Li H, Grossman JC (2017) Optically-controlled long-term storage and release of thermal energy in phase-change materials. *Nat Commun* **8**:1446. [Google Scholar](#)
23. †Han GGD, Deru JH, Cho EN, Grossman JC (2018) Optically-regulated thermal energy storage in diverse organic phase-change materials. *Chem Commun (Camb)* **54**:10722–10725. [Google Scholar](#)
24. †Koshima H, Ojima N, Uchimoto H (2009) Mechanical motion of azobenzene crystals upon photoirradiation. *J Am Chem Soc* **131**:6890–6891. [CrossRef](#) [PubMed](#) [Google Scholar](#)
25. †Cahill DG (2004) Analysis of heat flow in layered structures for time-domain thermoreflectance. *Rev Sci Instrum* **75**:5119. [CrossRef](#) [Google Scholar](#)
26. †Wang XJ, Ho V, Segalman RA, Cahill DG (2013) Thermal conductivity of high-modulus polymer fibers. *Macromolecules* **46**:4937–4943. [Google Scholar](#)

PDF

Help

27. †Shrestha R, et al. (2018) Crystalline polymer nanofibers with ultra-high strength and thermal conductivity. *Nat Commun* **9**:1664. [Google Scholar](#)
28. †Xie X, Dennison JM, Shin J, Diao Z, Cahill DG (2018) Measurement of water vapor diffusion in nanoscale polymer films by frequency-domain probe beam deflection. *Rev Sci Instrum* **89**:104904. [Google Scholar](#)
29. †Miao TF, et al. (2018) Chirality construction from preferred pi-pi stacks of achiral azobenzene units in polymer: Chiral induction, transfer and memory. *Polymers (Basel)* **10**:612. [Google Scholar](#)
30. †Han DH, Tong X, Zhao Y, Galstian T, Zhao Y (2010) Cyclic azobenzene-containing side-chain liquid crystalline polymers: Synthesis and topological effect on mesophase transition, order, and photoinduced birefringence. *Macromolecules* **43**:3664–3671. [CrossRef](#) [Google Scholar](#)
31. †Wu S, et al. (2010) Supramolecular bisazopolymers exhibiting enhanced photoinduced birefringence and enhanced stability of birefringence for four-dimensional optical recording. *J Mater Chem* **20**:5202–5209. [Google Scholar](#)
32. †Makhiyanov N, Temnikova EV (2010) Glass-transition temperature and microstructure of polybutadienes. *Polym Sci Ser A* **52**:1292–1300. [Google Scholar](#)
33. †Konstantinov VA (2011) Heat transfer in molecular crystals. *Heat Transfer—Theoretical Analysis, Experimental Investigations and Industrial Systems*. Available at <https://www.intechopen.com/books/heat-transfer-theoretical-analysis-experimental-investigations-and-industrial-systems/heat-transfer-in-molecular-crystals>. Accessed March 4, 2019. [Google Scholar](#)
34. †Velez C, Khayet M, de Zarate JMO (2015) Temperature-dependent thermal properties of solid/liquid phase change even-numbered n-alkanes: n-Hexadecane, n-octadecane and n-eicosane. *Appl Energy* **143**:383–394. [Google Scholar](#)
35. †Guo SF, Sugawara-Narutaki A, Okubo T, Shimojima A (2013) Synthesis of ordered photoresponsive azobenzene-siloxane hybrids by self-assembly. *J Mater Chem C Mater Opt Electron Devices* **1**:6989–6995. [Google Scholar](#)
36. †Seki T (2014) New strategies and implications for the photoalignment of liquid crystalline polymers. *Polym J* **46**:751–768. [Google Scholar](#)
37. †Hassan S, Anandakathir R, Sobkowicz MJ, Budhlall BM (2016) Tuning oxygen permeability in azobenzene-containing side-chain liquid crystalline polymers. *Polym Chem Uk* **7**:1452–1460. [Google Scholar](#)
38. †Bobrovsky A, et al. (2017) Photo-orientation phenomena in photochromic liquid crystalline azobenzene-containing polymethacrylates with different spacer length. *Macromol Chem Phys* **218**:1700127. [Google Scholar](#)
39. †Kang K, Koh YK, Chiritiescu C, Zheng X, Cahill DG (2008) Two-tint pump-probe measurements using a femtosecond laser oscillator and sharp-edged optical filters. *Rev Sci Instrum* **79**:114901. [CrossRef](#) [PubMed](#) [Google Scholar](#)
40. †Xie X, et al. (2017) High and low thermal conductivity of amorphous macromolecules. *Phys Rev B* **95**:035406. [Google Scholar](#)
41. †Li DY, Zhao P, Zhao JC, Cahill DG (2013) Generation and detection of gigahertz surface acoustic waves using an elastomeric phase-shift mask. *J Appl Phys* **114**:143102. [Google Scholar](#)

PDF

Help

42. O'Hara KE, Hu XY, Cahill DG (2001) Characterization of nanostructured metal films by picosecond acoustics and interferometry. *J Appl Phys* **90**:4852–4858. [CrossRef](#) [Google Scholar](#)
43. Shin J, et al. (2019) Data from “GIWAXS, GISAXS, WAXS and SAXS data for publication: Light-triggered thermal conductivity switching in azobenzene polymers.” Globus MDF Open. Available at dx.doi.org/doi:10.18126/M2VH2X. Deposited January 10, 2019. [Google Scholar](#)

We recommend

Correction for Shin et al., Light-triggered thermal conductivity switching in azobenzene polymers
National Academy of Sciences, *Proc Natl Acad Sci U S A*, 2019

Soft, skin-interfaced microfluidic systems with integrated immunoassays, fluorometric sensors, and impedance measurement capabilities

Sungbong Kim et al., *Proc Natl Acad Sci U S A*

Reversible photoswitching of encapsulated azobenzenes in water

Dipak Samanta et al., *Proc Natl Acad Sci U S A*, 2018

Ubiquitin S65 phosphorylation engenders a pH-sensitive conformational switch

Xu Dong et al., *Proc Natl Acad Sci U S A*, 2017

High thermal conductivity in soft elastomers with elongated liquid metal inclusions

Michael D. Bartlett et al., *Proc Natl Acad Sci U S A*, 2017

Atomic switches of metallic point contacts by plasmonic heating

Weiqiang Zhang et al., *Light: Science & Applications*, 2019

High-contrast and reversible polymer thermal regulator by structural phase transition

Ramesh Shrestha et al., *Sci Adv*, 2019

PHOTOPHYSICAL PROPERTIES OF LIGHT RESPONSIVE LIQUID CRYSTALS IN POLYMERIC TEMPLATES

World Scientific

Avelumab Maintenance Therapy for Advanced or Metastatic Urothelial Carcinoma

Thomas Powles et al., *NEJM*, 2020

High thermal conductivity in electrostatically engineered amorphous polymers

Apoorv Shanker et al., *Sci Adv*, 2017

Powered by **TREND MD**

PDF

Help

Next 

 Previous

 Back to top

 Article Alerts

 Email Article

 Citation Tools

 Request Permissions

 Share

Tweet

Like 1



ARTICLE CLASSIFICATIONS

Physical Sciences » Engineering

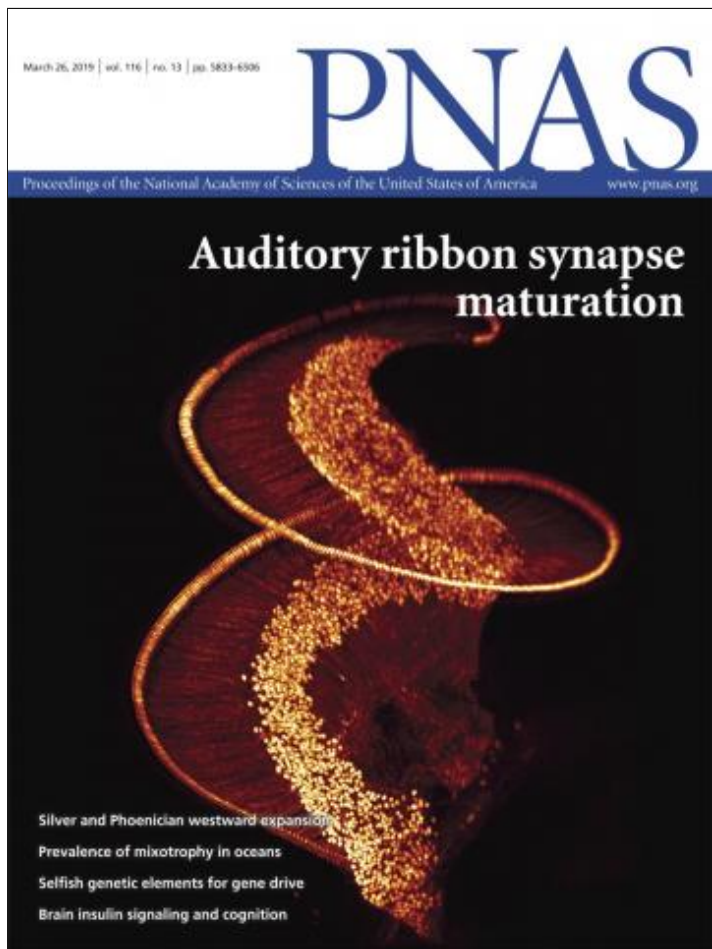


Table of Contents

Submit

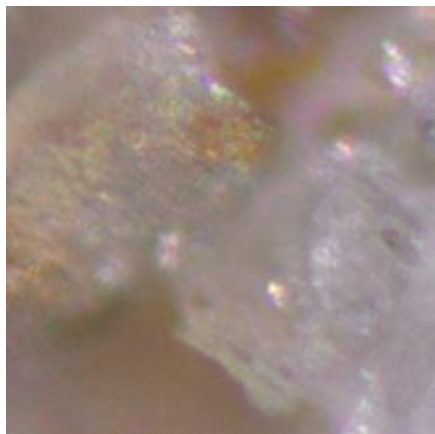
PDF
Help

Sign up for the PNAS *Highlights* newsletter to get in-depth stories of science sent to your inbox twice a month:

Sign up

✉ Sign up for Article Alerts

YOU MAY ALSO BE INTERESTED IN



Microplastics in the atmosphere

Even after atmospheric microplastics settle on land or in water, they may reenter the atmosphere, a study suggests.

Image credit: Janice Brahney.



Publicized racial violence and Black mental health

Researchers examine how highly public racial violence affects the mental health of Black individuals in the United States.

Image credit: iStock/fizkes.



Anthropogenic transformation of terrestrial nature

A study examines how humans have reshaped terrestrial nature and suggests that restoring Indigenous peoples and local communities to positions of environmental stewardship may help conserve biodiversity.

Image credit: Erle C. Ellis.

PDF

Science and Culture: The evolving portrait of a virus

Since start of the pandemic, depictions of the virus that causes COVID-19 have become iconic, visual touchstones for a nervous public.



Image credit: David Goodsell.



Journal Club: Mask-wearing may reduce the odds of self-infection with SARS-CoV-2

Working with members of the Deaf community to study people who don't vocalize, researchers find that droplets from one's own speech could contribute to infection.

Image credit: Shutterstock/insta_photos.

► Similar Articles

Correction for Shin et al., Light-triggered thermal conductivity switching in azobenzene polymers

Phase transition of RNA-protein complexes into ordered hollow condensates

High thermally conductive soft elastomer

Zintl-phase Eu_2ZnSb_2 : A promising thermoelectric material with ultralow thermal conductivity

Ultralow thermal conductivity in halide perovskite

PDF
Help
See more

 [Submit Manuscript](#)

 [Twitter](#)

 [Youtube](#)

 [Facebook](#)

 [RSS Feeds](#)

 [Email Alerts](#)

Articles

[Current Issue](#)

[Special Feature Articles – Most Recent](#)

[List of Issues](#)

PNAS Portals

[Anthropology](#)

[Chemistry](#)

[Classics](#)

[Front Matter](#)

[Physics](#)

[Sustainability Science](#)

[Teaching Resources](#)

Information

[Authors](#)

[Editorial Board](#)

[Reviewers](#)

[Subscribers](#)

[Librarians](#)

[Press](#)

PDF

Help

[Cozzarelli Prize](#)

[Site Map](#)

[PNAS Updates](#)

[FAQs](#)

[Accessibility Statement](#)

[Rights & Permissions](#)

[About](#)

[Contact](#)



[Feedback](#) [Privacy/Legal](#)

Copyright © 2021 National Academy of Sciences. Online ISSN 1091-6490. PNAS is a partner of CHORUS, COPE, CrossRef, ORCID, and Research4Life.

PDF

Help